CONCEPTUAL DESIGN OF POINTING CONTROL SYSTEMS FOR SPACE STATION GIMBALLED PAYLOADS

Robert O. Hughes
General Electric Space Division
Philadelphia, Pennsylvania

First NASA/DOD CSI Technology Conference
Norfolk, Virginia
November 18-21, 1986

CONCEPTUAL DESIGN OF POINTING CONTROL SYSTEMS FOR SPACE STATION GIMBALLED PAYLOADS

Robert O. Hughes
General Electric Space Division
Philadelphia, Pennsylvania

Abstract

A conceptual design of the control system for Payload Pointing Systems (PPS) is developed using classic Proportional-Integral-Derivative (PID) techniques. The major source of system pointing error is due to the disturbance-rich environment of the Space Station in the form of gimbal baseplate motions. These baseplate vibrations are characterized using Fast Fourier Transform (FFT) techniques. Both time domain and frequency domain dynamic models are developed to assess control system performance. Three basic methods exist for the improvement of PPS pointing performance: increase control system bandwidth, add Image Motion Compensation, and/or reduce (or change) the baseplate disturbance environment.

Introduction

A permanently manned Space Station (SS) is planned to be launched in the early 1990's and will orbit at about 460 Km and 28 1/2 degrees inclination. The current baseline configuration, the "dual keel" concept, is about 400 ft. long and is shown in Figure 1. The Station will orbit in a nadir pointing, gravity gradient orientation and an initial electrical power capacity of approximately 75 KW will be generated by a combination of photovoltaic solar arrays and point focusing collectors with heat engines. A central thermal heat rejection system for Attached Payloads using fluid loops and large articulating radiators is planned.

Of the approximately one hundred experiments/ instruments identified as candidate Attached Payloads for the Space Station, about forty per cent require some type of pointing capability. The accuracy requirements for these pointed payloads vary from sub-arc seconds to degrees and include several high technology solar and celestial telescopes. Most of these telescopes and other sky-viewing instruments will be mounted on the upper boom; the earth viewing payloads will be mounted on the lower boom.

Presented as paper 86-1986-CP at AIAA GN&C Conference, Williamsburg, Va., Aug. 18-20, 1986.

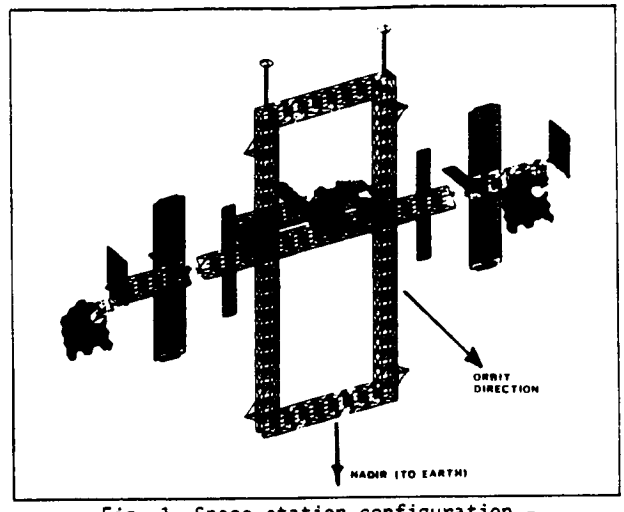

Fig. 1 Space station configuration - dual keel concept.

The Space Station attitude will be controlled by at least six large Control Moment Gyros (CMGs). Momentum build-up will be managed by off-nadir angles or Torque Equivalent Angles (TEA) generating desirable, momentum-dumping gravity gradient torques. Current estimates of the maximum nominal TEA are ± 5° in all axes with rates of .02°/sec per axis. Because the Space Station will not be stationary in its reference frame, generic and reusable pointing mounts are envisioned as the most cost-effective method of achieving most of the payload pointing requirements. These pointing mounts are called Payload Pointing Systems (PPS). Much analysis and design effort has been expended within the past decade on Shuttle based pointing mounts. Laskin and Sirlin[1] compare twelve different types of gimbal systems and perform technology assessments of actuators, sensors, isolation/suspensions systems, and control techniques. The European Instrument Pointing System (IPS) represents a type of design being considered for Space Station applications. IPS has a large payload capability (up to 7000 Kg) and has achieved in-flight sub-arc second pointing accuracies[2] during Shuttle/Spacelab quiescence disturbance periods. A major drawback of the IPS is its

end-mounted gimbal arrangement. Due to the center-of-mass offsets, this type of configuration is very sensitive to vibrational disturbances but is versatile in payload accommodation[3]. The disturbances created by normal crew activity during the Spacelab 2 mission caused pointing errors sizably larger than anticipated[4].

The Space Station as shown in Figure 1 represents a Large Space Structure (LSS). As there are no plans to either control the flexible modes (in an active distributed sense) or to estimate (observe) flexible vibrations for feed-forward reasons, non-trivial disturbances will exist at locations where gimballed payloads will be mounted. This base plate disturbance represents the major source of error for the gimbal control system. A typical CG gimbal concept is shown in Figure 2 and has a third axis of rotation which alleviates gimbal lock situations.

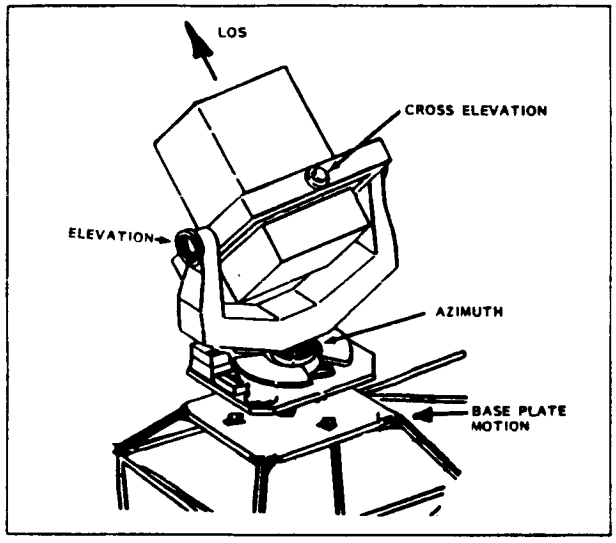

Fig. 2 CG- mount gimbal concept - 3 axes.

Disturbance Environment

Many internal and external forces will act on the Space Station causing the excitation of the lightly damped modal frequencies. The resulting vibrations at the mounting or base plate locations will be a major part of the pointing system's disturbance environment.

Disturbance Sources Smaller "ever-present" types of Space Station disturbances include: venting, slosh, machinery and pump vibrations, solar array and radiator motions, CMG torques, payload articulations, and console operations[5]. Larger disturbances occurring in a less random manner include: crew member kickoffs, nominal MRMS (Remote Manipulator) operations, tether operations, laboratory centrifuge operations, and astronaut treadmill activities. Very large disturbances occurring at very predictable and discrete points in time are Shuttle docking, RCS reboost (Station keeping via thrusters), and large excursions of the MRMS with massive payloads.

It has been determined that the maintenance of precision pointing during periods of large disturbances would not be cost-effective as the induced vibrations are more than thirty times larger than the other disturbance types. It is expected that these discrete occurrences will be coordinated with payload misssion timelines in order to minimize data loss. However, payload pointing capabilities must be maintained for the two smaller disturbance levels. These levels represent quiescence or background disturbance levels.

NASTRAN Model To investigate the effects of these background sources of excitation, a NASTRAN model of the Space Station was developed. Forcing functions that modeled a "standard" crew kick-off in the pressurized module, treadmill operations, and a centrifuge with a 20 pound mass imbalance were used as model inputs. Vibration levels were assessed at various locations on the SS where pointed payloads were likely to be attached, and a representative rotational/translational case was selected. This location turned out to be at the corner of the upper boom (see Figure 1) and Figure 3 shows the rotational motion.

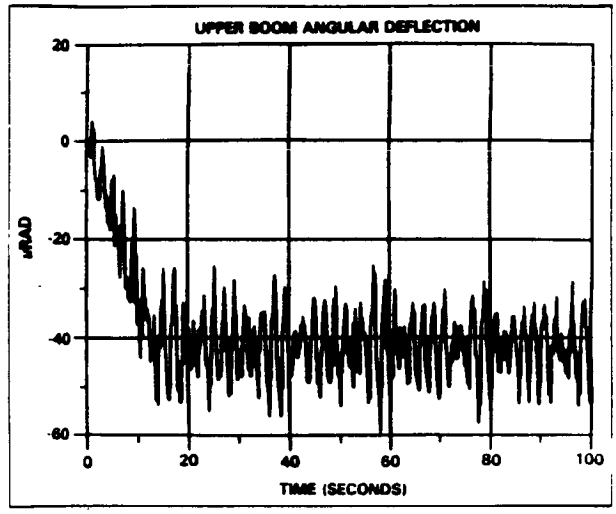

Fig. 3 Upper boom response to disturbances.

Effects of the crew kickoff causes a discernible displacement of approximately 40 microrad (8.3 arc-sec). High frequency vibrations are evident with maximum peak-to-peak variations of about 7.7 arc-sec.

Fast Fourier Transforms (FFT) The appropriate time history data files from the NASTRAN Model were processed using discrete FFT techniques[6]. The two FFT responses chosen for this study are shown in Figures 4 and 5 and represent baseplate rotational deflections and linear accelerations. The large responses at 1 Hz and 2 Hz are caused by the treadmill operation.

Control System Analysis

Models A simplified representation of the dynamic model used to assess pointing performance

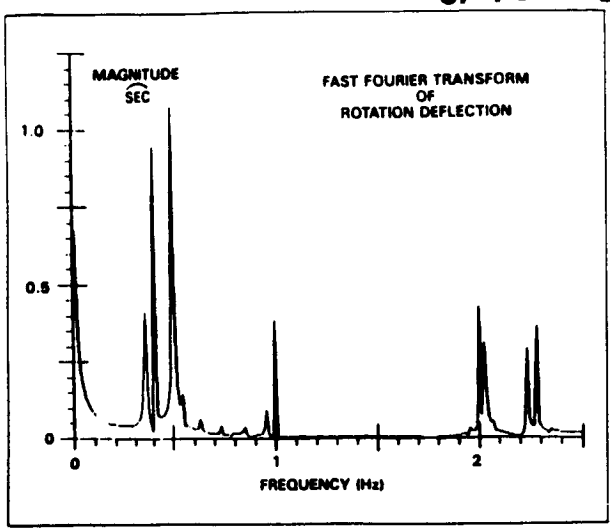

Fig. 4 Fast fourier transform (FFT) of disturbance response - rotation.

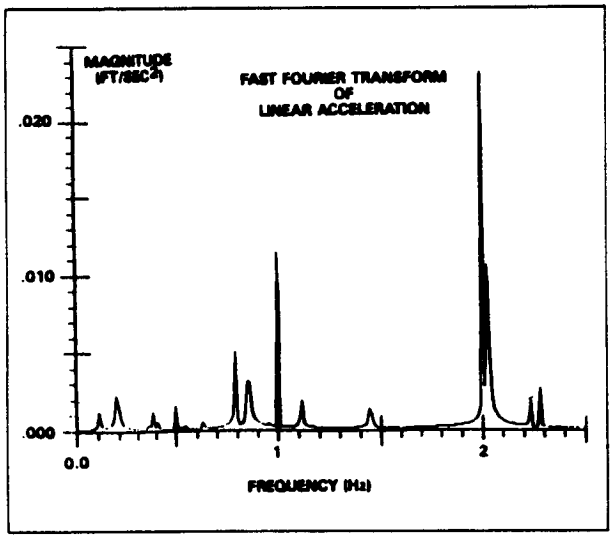

Fig. 5 Fast fourier transform (FFT) of disturbance response-linear acceleration.

of Payload Pointing Systems (PPS) is shown in Figure 6. The assumptions used in the derivation of this model include:

1) The payload was modeled as a uniform cylinder of mass M and length L. CG offsets, R, could vary from 0 (CG mount) to L/2 (end mount). The payload inertia, J, was calculated as a function of M, L, and R.

2) Frictional forces in the gimbal were modeled as a linear damping term, F. There were no non-linearities and no cable wrap-up torques.

3) The motor was modeled as a perfect torquer without time constants but with a saturation torque value of Tmax.

4) The system was noise-free and drift-free. Knowledge of the desired pointing direction was assumed perfect (implying an error-free payload sensor).

5) Only a single gimbal axis was modeled.

6) The controller was implemented in a perfect analog computer (i.e., no sampling problems).

7) The gimbal/payload was considered infinitely stiff except as noted in the flexibility discussions. No dynamic interactions with the SS were present.

8) Orbital velocity (about .06 deg/sec) was uniform, known, and used as a feed-forward input into the control system. This feed-forward technique transforms the tracking control problem into a regulator control problem[7] and results in lower problem pointing errors and increased stability margins.

Base plate vibrations represented by the two FFT responses were used as the disturbance inputs for the closed loop control system. The baseplate angular rotations (arc-sec) cause direct Line-Of-Sight (LOS) errors and must be corrected by opposing

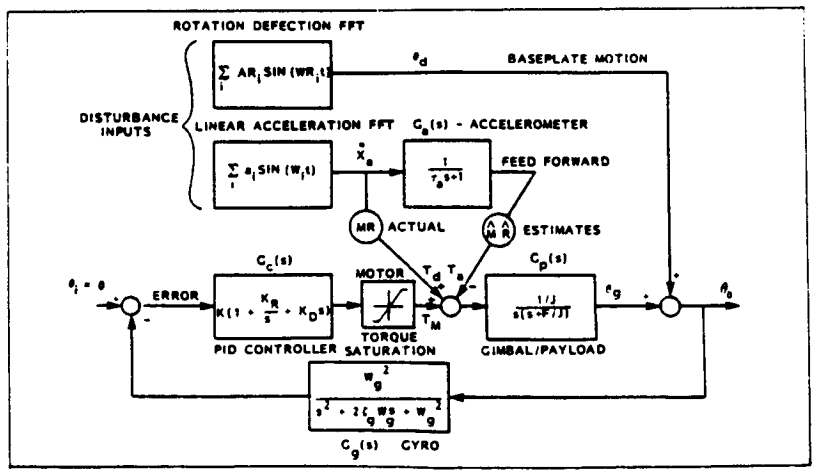

Fig. 6 Payload pointing system dynamic model.

C-5

gimbal motions. The linear accelerations $\ddot{X}_a(t)$ (ft/sec^2), act on the payload mass M (see Figure 7) through existing CG offsets, R, and cause a disturbance torque, T_d, about the gimbal axis.

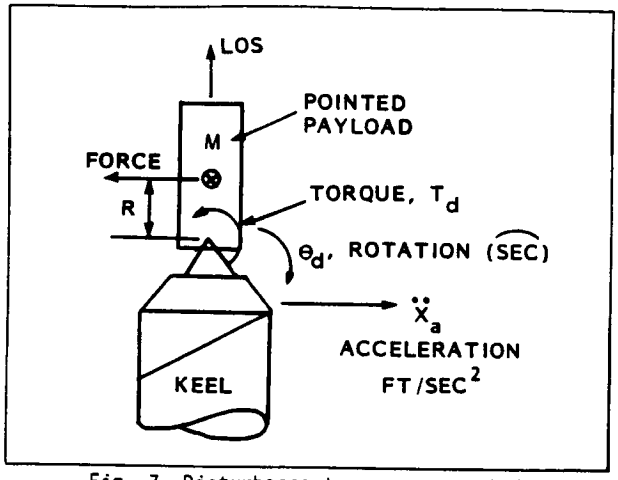

Fig. 7 Disturbance torques generated by CG-offsets.

A technique for counteracting this disturbance torque is accelerometer feed-forward compensation[8,9]. A properly oriented accelerometer with a transfer function of $G_a(s)$ measures the linear acceleration. Using estimates of payload mass, M, and CG offset, R, an opposing torque signal, T_a, is generated and used as an input to the control system. Major problems with this technique are: alignment, accurate estimates of M and R, noise, and the accelerometer's effective time constant, τ_a.

Controller Design The type of controller chosen for the conceptual design of the PPS is the classic Proportional - Integral Derivative (PID). This control design is not optimal and other techniques probably could provide higher performance; however, the PID design is well understood and provided needed versatility in the early stages of anlaysis.

To achieve a commonality in the performance assessment of various payloads, parameters, and disturbances, the pole placement technique of Guillemin-Truxal[10] was used to calculate the PID gains. That is, as various configurations and different size payloads were analyzed, the closed loop dominant poles were designed to remain in fixed positions. The three PID gains (K, K_r, and K_d) specified the locations of the two system zeros and the positions of the roots along the root locus. The controller zeros and the closed-loop poles are shown in Figures 8 and 9 for the nominal parameter values listed in Figure 10. These poles/zero locations dictate the bandwidth, stability margins, and pointing error performance of the control system.

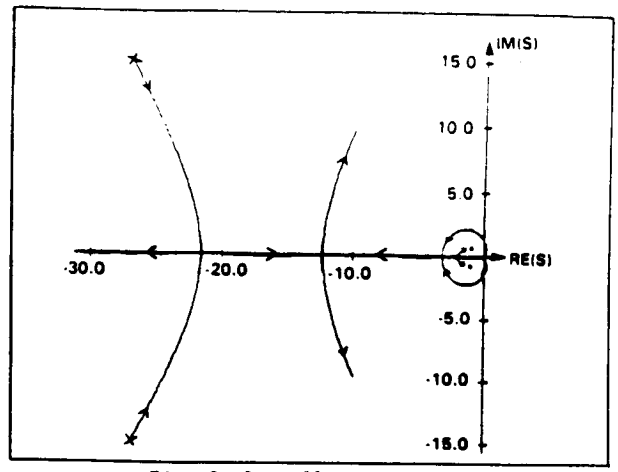

Fig. 8 Overall root locus.

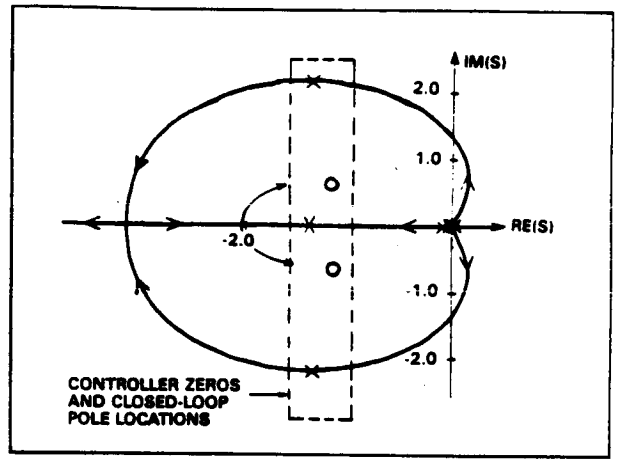

Fig. 9 Root locus-exploded view of dominant roots and controller zeros.

SYMBOL	NAME	UNITS	VALUE
M	Payload Mass	Kg	2000
L	Payload Length	m	3
R	CG Offset	m	0
J	Payload Inertia	slug-ft^2	1108
F	Linear Damping	ft-lb/r/s	100
ω_n	Closed Loop Natural Freq.	rad/sec	2.33
ζ	Closed Loop Damping Ratio	-	.5
TMAX	Motor Torque Saturation	Ft-lb	23
ω_g	Gyro Natural Freq.	rad/sec	31
ζ_g	Gyro Damping Ratio	-	.87
τ_a	Accelerometer Time Constant	sec	.008
PL	Real Axis Pole Location	-	1

Fig. 10 List of nominal parameters.

If the gyro dynamics and the torque motor saturation function in Figure 6 are neglected, then the closed-loop characteristic equation can be expressed as:

$$1 + G_c(s)\, G_p(s) = 0. \quad (1)$$

Using Laplace Block diagram algebra and the plant/controller parameters this equation becomes

$$s^3 + (F/J+KK_d/J)s^2 + Ks/J + KKr/J = 0. \quad (2)$$

For the general factored form of the characteristic equation of

$$(s + c)\,((s + a)^2 + b^2) = 0 \quad (3)$$

and using

$$\begin{aligned} a &= \zeta w_n \\ b &= w_n \sqrt{1 - \zeta^2} \\ c &= PL * a \end{aligned} \quad (4)$$

the PID gain expressions become

$$\begin{aligned} K &= J * (2 * PL * \zeta^2 * w_n^2 + w_n^2) \\ K_r &= J * (\zeta * PL * w_n^3)/K \\ K_d &= J * ((2 + PL) * \zeta * w_n - F/J)/K \end{aligned} \quad (5)$$

where ζ is the closed loop damping ratio and w_n is the closed loop natural frequency. PL specifies the relative position of the real third pole in relationship to the real parts of the two imaginary poles. In other words, ζ and w_n specify the locations of the dominant complex poles and PL (nominally equal to unity) dictates the position of the real axis root.

Time Domain Analysis A time simulation model for the system was developed and a typical time response using the FFT disturbances and the nominal parameters (Figure 10) is shown in Figure 11 for a CG offset of 5 cm. It can be seen that the baseplate motion varies between ± 5 arc-sec while the resulting LOS error is larger. The reason for this is due to the disturbance torques being generated by the 5 cm CG offset.

Frequency Domain Analysis The PPS pointing problem is amenable to frequency domain analysis because of the sinusoidal nature of the disturbance inputs (FFTs). In general, these techniques are much faster (computationally) and more precise than those using time simulation techniques. With reference to Figure 6 and using Laplace Transform Algebra, the closed loop transfer function, derived to perform stability analyses, is:

$$\frac{\theta_o(s)}{\theta_i(s)} = \frac{G_c(s)\, G_p(s)}{1+G_c(s)G_p(s)\, G_g(s)} \quad (6)$$

The relationship between the true LOS error and the two disturbances is:

$$E(s) = \frac{\theta_d(s) + G_p(s)(1-G_a(s))MR\ddot{X}_a(s)}{1+G_p(s)G_c(s)G_g(s)} \quad (7)$$

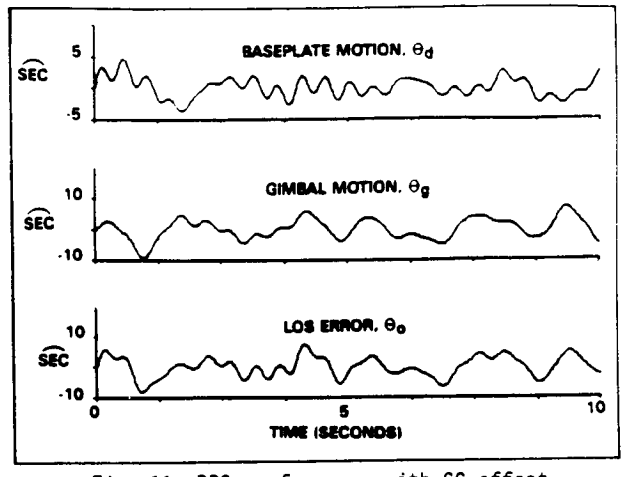

Fig. 11 PPS performance with CG-offset of 5 centimeters.

where perfect estimates of payload mass M and CG offset R are assumed. The true LOS error is

$$E(s) = \theta_i(s) - \theta_o(s) \quad (8)$$

and is slightly different than the measured error which has been modified by the gyro dynamics. Equation (7) can also be written as the sum of two error transfer functions. That is,

$$E_T(s) = E_1(s) + E_2(s) \quad (9)$$

where

$$E_1(s) = \frac{E(s)}{\theta_d(s)} = \frac{1}{1+G_p(s)G_c(s)G_g(s)} \quad (10)$$

and

$$E_2(s) = \frac{E(s)}{\ddot{X}_a(s)} = \frac{G_p(s)(1-G_a(s))MR}{1+G_p(s)G_c(s)G_g(s)} \quad (11)$$

$E_1(s)$ is the transfer function relating baseplate motion to LOS error. $E_2(s)$ represents additional error impacts due to CG offsets. Substituting jw for the Laplace variable s, the total LOS error can be calculated numerically as:

$$E = \sum_{i=1}^{N} AR_i(wr_i) * \left|E_1(jwr_i)\right| + \sum_{i=1}^{NR} A(w_i) * \left|E_2(jw_i)\right| \quad (12)$$

where w_i and wr_i are the FFT frequencies, A_i and AR_i are the FFT amplitudes, and N and NR are numbers of FFT frequencies considered. It should be noted that equation

(12) represents a maximum worst case condition because the error contributions at each frequency are added. From a time domain viewpoint, this scenario means that the maximum error occurs when all the FFT sine waves are at their peaks (i.e., pure constructive interference).

The functions $E_1(w)$ and $E_2(w)$ of equation (12) can be termed "Control System Attenuation Functions" and they represent how well the gimballed control system can handle the disturbance sinusoids. These functions are shown in Figure 12 and are for a CG offset of 5 cm and no accelerometer feed-forward compensation. Multiplying the FFTs by their corresponding attenuation functions, weighted FFTs will result. The summing of the values of the weighted peaks is the calculation performed by equation (12).

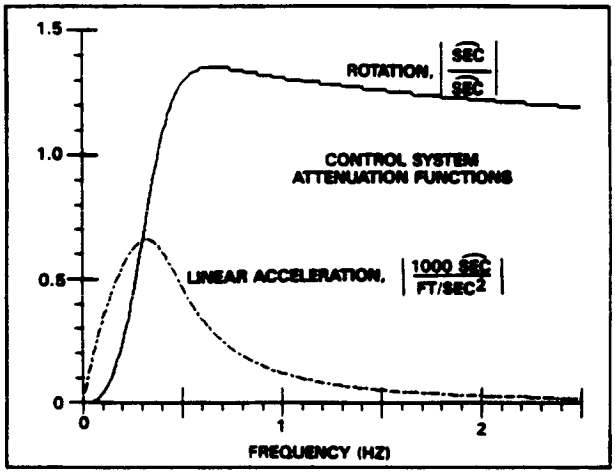

Fig. 12 Attenuation functions without feed-forward.

Bandwidth Considerations

One of the most important and descriptive parameters of a control system is its bandwidth. In general, bandwidth (or passband) is the range of frequencies that can pass through a control system. "High" bandwidth systems have fast response times and high performance factors but usually suffer from high frequency noise and reduced stability margins. "Low" bandwidth systems, while slower in reaction times, have excellent noise rejection characteristics. Laser Pointing Systems[11] have bandwidths above 100 Hz while spacecraft attitude control systems typically have bandwidths of .05 Hz and lower.

Many factors impact the bandwidth of a system[3] and include: controller design, structural flexibilities, nonlinearities, component bandwidths, component noise characteristics, and gain/phase stability margin specifications. An example of the difficulties in achieving high bandwidths was the Sperry-designed Advanced Gimbal System (AGS). Initially, an optimistic goal for a 2.4 Hz bandwidth was set. However, due to the combined effects of structural flexibility, gyro and accelerometer bandwidths, transport lags, and sampling effects, a control bandwidth of .7-1.3 Hz was achieved[12]. Bandwidths in this range appear reasonable for the PPS.

It is important to have a standard definition of bandwidth in order to compare different systems. The traditional and most widely accepted definition is "the -3db point of the closed-loop Bode Plot"[10,13]. In some systems[14], for example, the open loop crossover frequency is near the closed-loop -3db point and the two can be used interchangeably. Sometimes the natural frequency, w_n, of the dominant closed loop poles is referred to as the bandwidth. However, for the PPS system being considered herein, neither of these bandwidth definitions are correct.

Error vs. Bandwidth Variations in pointing error or stability error are shown in Figures 13 and 14 for different bandwidths, various CG offsets, and three different types of magnitude/frequency disturbance inputs. Figure 13 is the nominal case for a CG mount with small perturbing CG offsets. It is estimated that there will be a ± 5 cm CG uncertainty on orbit even with the use of an on-line mass balancing system. Without such a balancing system, an error of about ± 20 cm is estimated.

Large error sensitivities to different disturbances are seen in Figure 14. The term "8 Frequencies" indicates the nominal case of eight FFT frequencies for the rotation and acceleration disturbances. The term "3 frequencies" indicates that only the first three of the eight FFT frequencies were retained, and "1 frequency" means that only one frequency for each disturbance was used as an input. For the nominal case, the large errors which are relatively insensitive to bandwidth changes are caused by the high frequency disturbances outside the control system bandwidth. For the "3 frequency" case, bandwidth changes affect the error more strongly. The single frequency case was used to emphasize the importance of the magnitudes and frequencies FFT disturbances on pointing performance and as a verification tool. In this special configuration one frequency ($w = 1.97$ Hz with an amplitude of .023 ft/sec^2) from the acceleration FFT and one frequency ($wr = .51$ Hz with an amplitude of 1.08 arc-sec) from the displacement FFT were used as disturbances. A pointing error of ± 3.54 arc-sec resulted and is almost a four-fold improvement in pointing performance over the nominal disturbance case. This configuration served as a verification case as the time-varying pointing error generated by the time domain simulation model was virtually periodic over the simulation time and the maximum peak-to-peak variation could be measured with accuracy. There was less than a 1% error between values calculated by the frequency and time domain techniques.

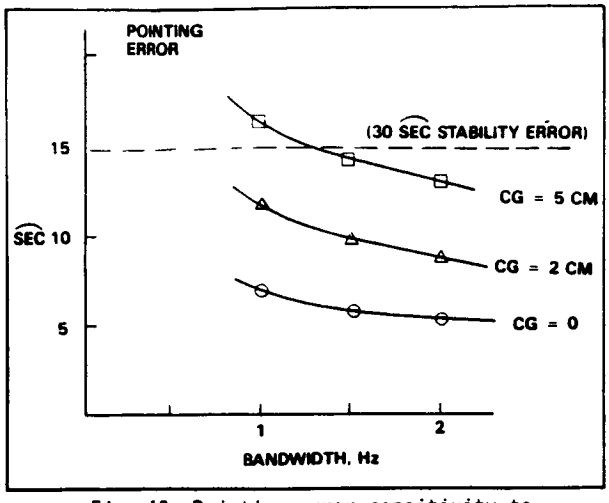

Fig. 13 Pointing error sensitivity to bandwidth and small perturbing CG offsets.

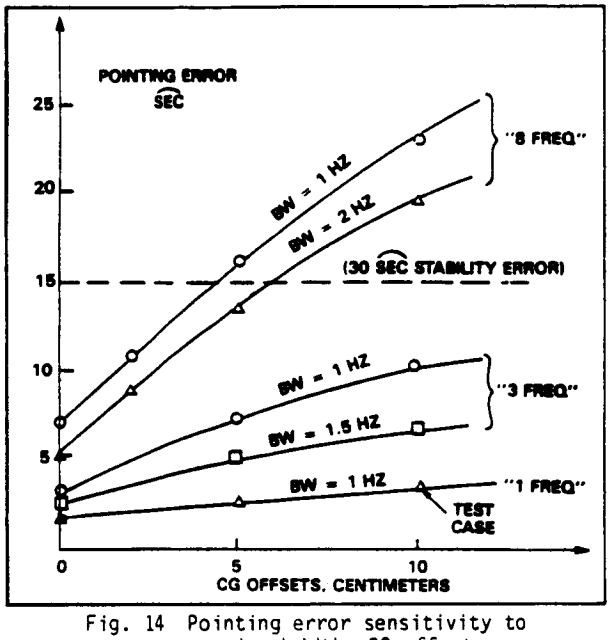

Fig. 14 Pointing error sensitivity to bandwidth, CG offset, and disturbance input.

Gyro Dynamics The dynamic characteristics of the gyro impact the overall control loop bandwidth and gain/phase margins. In Figure 15 Bode plots for three gyro natural frequencies are shown. The gain and phase margins for these cases are:

Wg (r/s)	GM (db)	PM(deg)
15	17	32
31	22	38
62	29	46

Hence, if a high gyro natural frequency (which is a measure of its bandwidth) can be realized, then higher control loop bandwidths can be achieved for the same gain/phase margins.

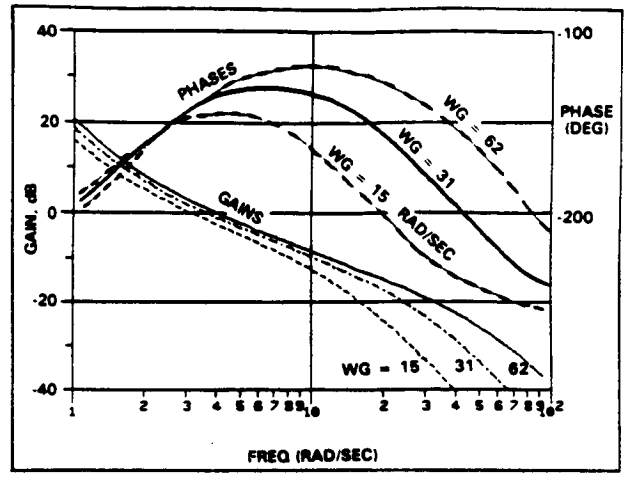

Fig. 15 Bode plots for three gyro bandwidths.

Feed-Forward Techniques Feed-forward methods can improve pointing performance without increasing the loop bandwidth. For example, if there were good predictions of the base plate motion generated by an on-board SS dynamic computer model, then these signals could drive the gimbals in phase, rather than having to wait for the sensors to detect errors.

A technique used in IPS and elsewhere is accelerometer feed-forward. Linear accelerations are sensed at the base plate and multiplied by estimates of the mass, M, and CG offsets, R. This generates a disturbance torque estimate and is used as an input to the control system. Problem areas of this technique include: noise and finite bandwidths of accelerometers, accurate mass and CG offset estimates, and sensitivity of the disturbance torques to gimbal angles. Assuming that the dynamics of the accelerometer can be approximated by a single time constant, τa, Figure 16 shows variations of pointing errors as functions of CG offsets and accelerometer break frequency ($1/\tau a$). Note that for this perfect, single-axis feed-forward method, the pointing error approaches that of an ideal CG mount as the bandwidth of the accelerometer approaches infinity. This also means that the accelerometer transfer function, $G_a(s)$, approaches unity and a perfect cancellation of the induced disturbance torques is acheived.

Flexibility Effects The effects of mechanical flexibility can have major impacts on the stability, performance, and bandwidths of pointing control systems. Flexible modes that are close to the control bandwidth will reduce gain/phase margins (similar to the previous gyro analysis) and could cause instability. Sometimes an increase in system bandwidth excites flexible modes which introduces larger pointing errors than experienced with smaller bandwidths[15].

In general, it is desirable from a control standpoint to make the gimbal/yoke structure as stiff as possible, thereby ensuring high modal frequencies. For example, in the

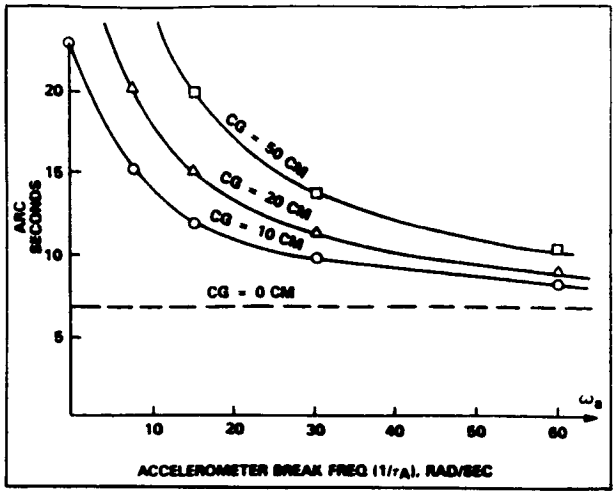

Fig. 16 Accelerometer time constant effect on pointing error.

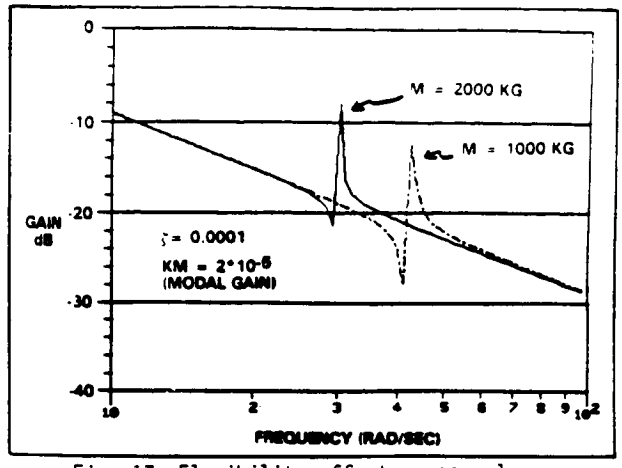

Fig. 17 Flexibility effects - open loop Bode (gain) plots.

early design phases of the AGS, a minimum frequency of 20 Hz was specified[16]. Refined numbers for structural stiffness, inertias, and damping are usually not available in the conceptual design phase of a project. Therefore, the overall control system design must be robust enough to accommodate changes in modal parameters. In the course of the IPS design, it was discovered that early stiffness estimates were too high and modifications to the control laws were necessary[17].

A general rule of thumb[18] for the design of a control system with potential flexibility problems is to choose the open-loop crossover frequency with about one-third the frequency that is not necessary to control. Another technique[8] is to design for a "minimum bandwidth" which provides for the maximum levels of margin while still meeting performance requirements.

The pole placement technique used in this study of the controller conceptual design assumed that the payload was a lumped inertia and effects of gimbal/yoke stiffness were not directly considered. Little difference in responses will be discerned for two payloads with different inertias as the loop gain, K, will increase linearly with the load inertia, J. In reality, this is incorrect as a large inertia will result in a low destabilizing fundamental frequency. Additionally, a high electrical loop gain will amplify the effects of system noise and will degrade performance. To demonstrate the effects of flexibility on loop stability, a single modal frequency transfer function was added in parallel to the payload block in Figure 6. The results of this simplified technique are shown in the open loop Bode Plot (Figure 17) for two payload masses (1000 Kg and 2000 Kg). Note that for the lower mass the resonant frequency has increased thereby providing about 6 db additional gain margin.

Options for Pointing Performance Improvement

As detailed in the previous sections the expected dynamic disturbances from the SS acting through traditional control systems with bandwidths of about 1 Hz will cause non-trival pointing errors; and, in some cases, a payload's pointing error requirement can be exceeded. The following is a discussion of several options that have potential for the improvement of pointing performance:

Controller Design Moderate improvements in pointing performance can be realized through optimal control design techniques or a more rigorous classical design approach. By advancing the state-of-the-art in sensor and actuator technologies[1], higher bandwidths can be achieved with smaller pointing errors as demonstrated in Figure 14.

Added Structural Damping An increase in the SS structural damping will decrease the amplitudes of the disturbance vibrations and a corresponding decrease in pointing error will result. Passive damping methods[19] appear promising. Active structural damping such as piezoelectric techniques are probably not cost-effective for the current SS design.

Image Motion Compensations (IMC) This proven technique is usually an integral part of an instrument's control design[20,21], but IMC also could be exterior to a payload[22]. Basically, IMC entails high bandwidth systems that control low mass actuators such as mirrors. The net effect of an IMC system is attenuation of the disturbance frequencies passed by the gimbal control system.

Disturbance Management Internal vibration sources of the space station can be managed in a fashion similiar to that of a spacecraft's traditional weight and power allocation/budget. Vibration absorbers and/or isolators can be added to equipment with offending disturbance spectra.

Payload Isolation This method attempts to isolate the pointed payload from the disturbance source which is, in this case, the entire space station. There are three isolation options to be considered: passive, active, and softmount.

Passive isolation, which typically uses springs and dampers, suffers from practical problems and does not appear feasible for the space station applications. To attenuate the > 1 Hz frequencies, an isolator frequency of .1 Hz or less would be required. For a 2000 Kg payload, this corresponds to a spring rate of 790 N/M which is likely to be softer than the power and thermal connections to and from the payload. Additionally, the gimbal system will not be able to react torques against the massive space station and this will introduce additional pointing errors. It is also likely that without any payload momentum compensation devices closed-loop stability problems will exist.

Magnetic suspension[23] and the Gimbalflex[24] are common techniques of active vibration isolation that have SS applicability. Typically, a magnetic suspension system will have six-degrees of freedom (three rotations and three translations) and will perform significantly better than passive devices[23]. The transfer of services across the isolator interface remains a problem for both types of active isolation in achieving adequate disturbance rejection.

The softmount[25] is a concept in which the payload becomes a virtual free-flyer with almost no dynamic interaction with the base body. The payload would require its own attitude control system using CMGs or reaction wheels and would be loosely connected to the space station via tethers or guy wires.

An example of how an idealized isolator in the form of a softmount could modify the error attenuation characteristics of the system considered in this study is shown in Figure 18. The example assumes: no dynamic interation between the gimbal control system and the isolator, payload pointing is controlled by CMGs with a 1 Hz bandwidth, and that all connections to the payload are such that the isolator system has a natural frequency of .1 Hz. The resultant isolator/control characteristic is similiar to that derived in a previous study[26] and provides for an order-of magnitude reduction in pointing error.

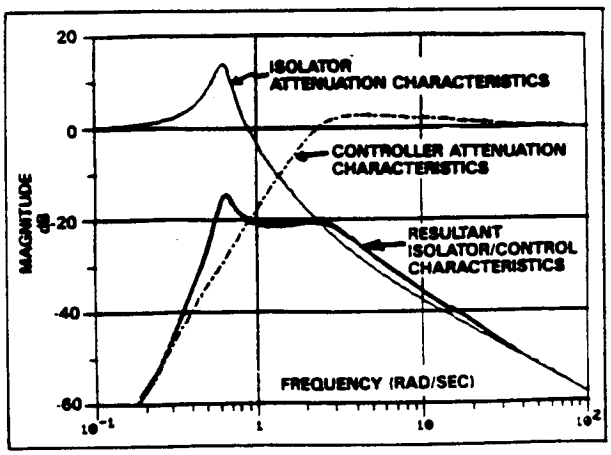

Fig. 18 Idealized isolation

CONCLUSIONS

A study of interface problems between the Space Station Structure and the Payload Pointing Control System has been completed. A major result is that the Space Station will have a disturbance-rich environment and vibration background levels will be large enough to impact the pointing performance of some payloads.

The dynamic model used to quantify the pointing performance of the conceptual design of the PPS included many simplified assumptions. It is expected that larger pointing errors will be observed when more detailed and accurate models of the PPS are developed.

End mounted gimbal systems suffer from CG offset problems and a CG mount is better from a pointing standpoint. It has been determined that at least a ± 5 centimeter CG offset will exist for a spaceborne CG mount even with an on-board mass balancing system.

To reduce the impact of Space Station vibrations on pointing performance, several design options were presented. The two most cost effective techniques appear to be disturbance management and payload Image Motion Compensation.

References

1. Laskin, R. and Sirlin, S., "Future Payload Isolation and Pointing System Technology," 1984 Position Location and Navigation Symposium, San Diego CA, Nov. 1984.

2. Hamesfahr, A., "The SpaceLab Instrument Pointing System Performance and Operations," AIAA Paper No 85-6073-CP, Shuttle Environment and Operations II Meeting, Houston, TX, Nov. 1985.

3. Hamilton, B., "Magnetic Suspension: The Next Generation in Precision Pointing," Proc. Rocky Mountain Guidance and Control Conference, Paper AAS 82-034, Feb. 1982.

4. "Spacelab 2 Scientists Fear Pictures Damaged", Aviation Week & Space Technology, p 21, Aug. 19, 1985.

5. Mettler, E., et. al., "Space Station On-Orbit Identification and Performance Monitor," paper AIAA 85-0357, 23rd Aerospace Sciences Meeting, Reno, Nevada, Jan. 1985.

6. Rabiner, L. and Rader, C., eds., Digital Signal Processing, IEEE Press, 1972.

7. Hughes, R.O., "Optimal Control of Suntracking Solar Collectors," Journal of Dynamic Systems, Measurement, and Control, Vol 101, June 1979.

8. Walton, V., "Fine Pointing Control of Orbiter Based Gimballed Payloads," Paper 77-1091, AIAA Guidance and Control Conference. Hollywood, FL, August 8-10, 1977.

9. Kösters, B, Thieme, G., and Müller, T., "Design of the IPS Control Loops," Automatic Control in Space, 8th Symposium, Oxford, England, July, 1979.

10. D'Azzo and Houpis, Linear Control System Analysis and Design, McGraw Hill, 1975.

11. Deadrick, R., "Design and Performance of a Satellite Laser Communications Pointing System," Paper AAS 85-016, Proc. Rocky Mountain Guidance and Control Conference, 1985.

12. "Advanced Gimbal System Critical Design Review," Sperry Flight Systems, April 14, 1982.

13. "Design of the Annular Suspension and Pointing System (ASPS)," Sperry Flight Systems, NASA Contractor Report 3343, Oct. 1980.

14. Åström, K. and Hägglund, T.," A Frequency Domain Method for Automatic Tuning of Simple Feedback Loops," IEEE CDC Conference, Las Vegas, NV, Dec. 1984.

15. Keckler, C.," High Accuracy Pointing for Earth Observations Experiments," Paper 84-1880, Guidance and Navigation Control Conference, Seattle, Wash., 1984.

16. Shelton, H., et. al., "Effects of Flexibility on AGS Performance," Paper AAS 82-002, Proc. Rocky Mountain Guidance and Control Conference, 1982.

17. Thieme, G., et. al., "Sampled Control Stability of the ESA Instrument Pointing System," IFAC Automatic Control in Space, 1982.

18. Nesline, F. and Zarchay, P., "Why Modern Controllers Can Go Unstable in Practice," AIAA Journal of Guidance and Control, Vol 7, No. 4., July, 1984.

19. Ashley, H., "On Passive Damping Mechanisms in Large Space Structures," Journal of Spacecraft, p 448, Sept. 1984.

20. Lorell, K. et. al., "Internal Image Motion Compensation System for the Shuttle Infrared Telescope Facility," Automatic Control In Space, 8th Symposium, Oxford, England, July, 1979.

21. Gowrinathan, S. and Gottesman, J., "Articulated Primary Mirror (APM) for the Solar Optical Telescope (SOT)," SPIE Vol. 265 Supplement, 1981.

22. Shelton, H., "Image Motion Compensation for the OSS-3/7 Telescopes," Paper AAS 83-006, Proc. Rocky Mountain Guidance and Control Conference, 1983.

23. Havenhill, D. and Kral, K., "Payload Isolation Using Magnetic Suspension," Paper 85-014, Proc. Rocky Mountain Guidance and Control Conference, 1985.

24. Osborne, N., "Gimbalflex 5-Degree of Freedom Inertially Stabilized Platform," Paper AAS-80-015, Proc. Rocky Mountain Guidance and Control Conference, 1980.

25. Sirlin, S. and Laskin, R., "Payload Isolation and Precision Pointing for the 1990's," Paper 85-010, Rocky Mountain Guidance and Control Conference, 1985.

26. Hamilton, B., "Stability of Magnetically Suspended Optics in a Vibration Environment," Sperry Flight Systems Pub 69-1554-02-00, June, 1981.